Published in final edited form as:
J Magn Reson Imaging. 2010 November ; 32(5): 1054–1060. doi:10.1002/jmri.22381.

Effects of Formalin Fixation on Magnetic Resonance Indices in Multiple Sclerosis Cortical Gray Matter

Klaus Schmierer, PhD[1,2,*], **Janet R. Thavarajah, MSc**[1], **Shu F. An, PhD**[3], **Sebastian Brandner, MD**[3], **David H. Miller, MD**[1], and **Daniel J. Tozer, PhD**[1]

[1]UCL Institute of Neurology, Department of Neuroinflammation, NMR Research Unit, London, United Kingdom.

[2]Barts and the London School of Medicine & Dentistry, Blizard Institute of Cell and Molecular Science, Centre for Neuroscience & Trauma, London, United Kingdom.

[3]UCL Institute of Neurology, Division of Neuropathology, London, United Kingdom.

Abstract

Purpose—To investigate changes in magnetic resonance imaging (MRI) indices following formalin fixation of postmortem multiple sclerosis (MS) cortical gray matter (CGM). Postmortem MS brain is being used to establish pathological correlates of changes detected using MRI, with recent emphasis on CGM. Fixation induces tissue alterations that may confound inference of in vivo observations from MRI/histology correlation studies.

Materials and Methods—T_2-weighted scans were obtained alongside quantitative T_1, magnetization transfer ratio (MTR), and macromolecular proton fraction (f_B) measurements before and after formalin fixation of 15 postmortem brain samples. Type and size of CGM lesions (CGML) was identified on sections immunostained for myelin basic protein.

Results—MRI indices obtained in unfixed MS CGM were similar to values obtained in subjects with MS in vivo. Fixation led to reduction in T_1 (617 msec [standard deviation = 114] vs. 1156 msec [216]) and MTR (24.1 [3.3] percent units [pu] vs. 29.1 [2.5] pu) and increase in f_B (5.4 [0.7] pu vs. 3.2 [2.3] pu) (all $P < 0.01$). The proportion of CGM affected by demyelination did not alter the MRI data.

Conclusion—MRI indices in the CGM are significantly altered following tissue fixation.

Keywords

multiple sclerosis; postmortem; fixation effects; cortex; cortical lesions; magnetization transfer; T1

INTRODUCTION

Multiple Sclerosis (MS) is an inflammatory and degenerative disease of the central nervous system (CNS) (1). Magnetic resonance imaging (MRI) is currently the most important tool to confirm the diagnosis of MS (2), to rule out differential diagnoses (3), and to assess the effect of novel treatments in phase II and phase III clinic trials for MS (4).

[*]Address reprint requests to: Klaus Schmierer, Barts and the London School of Medicine & Dentistry, Department of Neurology, 4th Floor, Holland Wing, The Royal London Hospital, London E1 1BB, UK. k.schmierer@qmul.ac.uk.

Europe PMC Funders Author Manuscripts

Postmortem MS brain can be used to establish the pathological correlates of changes detected using MRI (5). Studies using this approach have successfully underpinned the development of MRI markers relevant to MS. For example, the recovery of magnetization transfer ratio (MTR) and of myelin water fraction from multicomponent T_2 in MS white matter (WM) lesions (WML), as well as the evolution from hypo- to isointensity of WML detected on T_1-weighted (T_1w) scans have all been endorsed as indices of remyelination (4) (an important repair mechanism in MS (6)) following validation of these MR measures in correlative MR/histology studies using postmortem MS brain (7,8). Hence, MR/histology correlation studies using postmortem brain may directly impact on the use (and usefulness) of MR indices in patients with MS in vivo, for example, in clinical trials of putative agents that enhance remyelination.

Formalin fixation, however, introduces chemical alterations of tissue with potential to confound inference of in vivo observations from MR/histology studies (10). Effects of fixation on quantitative MR indices in MS WM have been reported (11). However, fundamental differences in the cellular (12) and biochemical (13) composition between cortical gray matter (GM) and WM could result in a different impact on the changes these tissue compartments undergo when exposed to fixation. In this study we specifically investigated changes in MS cortical GM (CGM) following fixation of the quantitative MR (qMR) indices T_1, MTR, and fraction of macromolecular protons (f_B).

MATERIALS AND METHODS

Patients/Samples

This study was approved by the Ethics Committee. MRI datasets and paraffin-embedded tissue blocks were used from 15 postmortem brain slices that had been donated by 14 women and one man with MS to the UK Multiple Sclerosis Tissue Bank (MSTB) based at Imperial College London. In each case a coronal brain slice (≈1 cm thick) from one hemisphere was dissected in unfixed condition at the level of the mammillary bodies. The brain slices used were collected from the MSTB within a mean of 17 (standard deviation [SD] = 6) hours postmortem. Clinical information including age, disease duration, date and time of death were obtained from the case records, held at the MSTB. The degree of disability was estimated from the case records, and an “estimated” expanded disability status scale (eEDSS) score calculated. MRI datasets and tissue blocks used in this study had been used previously to investigate WM changes following fixation (11).

Prior to the first scanning session the unfixed postmortem brain slices were kept in plastic bags and stored in a refrigerator at ≈2–8°C. Several hours before scanning they were taken out of the refrigerator and the plastic bags, wrapped in polyethylene film to retain moisture, and left to reach scanner room temperature. Brain slices were then scanned in unfixed condition 51 hours (SD = 28 hours) after death. Following this first scanning session, the samples were immersed in 10% buffered formalin and kept at room temperature. Following an interval of 64 (SD = 42) days brain slices were rescanned in fixed condition. For this purpose the samples were removed from their formalin bath and again wrapped in polyethylene film to prevent drying. The temperature of the slices was measured immediately following each scanning session using a thermocouple thermometer (HI 93551) connected to a penetration probe (HPT1) from Hanna Instruments (Leighton Buzzard, Bedfordshire, UK).

MRI Scanning and Parameter Map Calculation

MRI was performed with a GE Signa Horizon Echospeed 1.5T system (General Electric, Milwaukee, WI) using a birdcage head coil. The MRI plane was positioned parallel to the

coronal surface and in the center of each brain slice. The following datasets were acquired using an imaging slice thickness of 5 mm, a field of view (FOV) of 24 × 24 cm^2 and a matrix size of 256 × 256 (resulting in a pixel size of 0.94 × 0.94 mm^2):

- 2D dual spin-echo (SE) proton density (PD)- and T_2-weighted (T_2w) images with parameters TR = 2000 msec and TE = 30/120 msec, respectively. These images were acquired in all 15 cases before and after fixation.
- 2D PD and T_1w gradient echo images TR/TE/ flip angle = 1500/11 msec / 45° and 36/11 msec / 45°, respectively), from which T_1 maps were generated as previously described (7,14). These data-sets were acquired in unfixed condition in all 15 cases, but only in 14 after fixation.
- 2D dual SE images (TR/TE1/TE2 = 1720/30/80 msec) obtained with (M_{sat}) and without (M_0) a sinc-shaped saturation prepulse applied 1 kHz off-water resonance, from which MTR maps were calculated according to MTR = 100 × (M_0–M_{sat})/M_0 (15). These datasets were acquired in all 15 cases before and after fixation.
- 2D spoiled gradient echo images (TR/TE / flip angle = 1180/12 msec / 25°; FOV = 240 × 180 mm with partial *k*-space coverage, reconstructed as 256 × 256 over a 24-cm FOV). A Gaussian MT pulse of 14.6 msec duration was applied with 10 different combinations of MT pulse offset and power (three powers were used) as previously described (11,16). This allows quantitative analysis of the MT phenomenon using the model described by Henkelman et al (17) with modifications by Ramani et al (18) to allow for pulsed rather than continuous MT saturation. The model allows calculation of six parameters (R_{1B}, RM_{0A}, gM_{0A}, f_B/$R_{1A}(1 - f_B)$, $1/R_{1A}T_{2A}$, and T_{2B}). These are combinations of the fundamental parameters f_B, R_{1A}, and R_{1B} (the inverse of the T_1 of the A [free water proton-] and B [macromolecular proton-] pools, respectively), R (the time constant for the interaction for the two proton pools), T_{2A} and T_{2B} (their transverse relaxation times), M_{0A} (the initial magnetization of the A pool), and g (the scanner gain). With the separate measurement of R_1 from the T_1 maps described above, f_B can be extracted. However, the independent determination of other interlinked parameters is not possible. Analysis of the acquired data was performed as previously described (16). These datasets were acquired in eight cases before and after fixation.

Cortical Gray Matter Segment Production

MR scans were displayed on a Sun workstation (Sun Microsystems, Mountain View, CA) using DispImage (19). Cortical GM masks were then produced of each case as follows: On the T_2w image of the brain slice in unfixed condition (Fig. 1a) three regions of interest (ROIs) were placed in the cortical GM (Fig. 1b), and the mean and SD of these three ROIs calculated. Areas of non-CGM and WML were marked (Fig. 1c) and removed (Fig. 1d) to avoid potential contamination of cortical GM maps. The T_2w images were then thresholded using the GM mean plus a multiple of the SD (usually 2; range 1–5) to produce cortical GM masks (Fig. 1e). The number of SDs used was chosen on a case-by-case basis to ensure that the final map includes as much cortical GM as possible while any other tissue component potentially contaminating the “pure” cortical GM mask is excluded; this final step was achieved by an iterative interactive manner with the user inspecting the results and varying the number of SDs used. The cortical GM mask was then applied to the qMR maps (T_1, MTR, f_B) of the same case to obtain mean values of the qMR indices (Fig. 1F) of cortical tissue. Cortical GM masks of MRI acquired after the brain slices had been fixed were produced, and then applied to the respective qMR maps, in the same way as described in unfixed cases.

In order to ensure that a similar volume of cortical GM was covered by masks produced on the basis of MRI acquisitions before and after tissue fixation, the CGM volumes were measured. Given that some degree of tissue deformation, including volume change, may occur as a result of the fixation process a difference of 10% between pre- and postfixation masks was deemed acceptable (20). If the volumes were not within the 10% tolerance the number of the SDs used at the thresholding stage (see above) was adjusted until this was achieved.

Histology

A total of 48 paraffin-embedded tissue blocks were available from the 15 brain slices. Sections of 5-μm thickness were obtained and stained with hematoxylin and eosin (H&E). Immunohistochemistry was run on Bond-Max (Vision Biosystems, Hemel Hempstead, UK). The primary antibody used was antimyelin basic protein (MBP, 1:1000, 60 minutes, room temperature, Covance, Cambridge Bioscience, Cambridge, UK) for myelin.

Histological analysis was performed using Image Pro Plus, v. 6.2 software (Media Cybernetics, Bethesda, MD) installed on a PC, which received its signal through a KY-F550E color video camera (JVC) mounted on a Zeiss Axioscope microscope (Carl Zeiss, Göttingen, Germany).

Cortical demyelination was identified on MBP stained sections as clearly distinct, sharply demarcated areas of myelin loss. Using a slightly modified classification system described previously (21), cortical demyelination was distinguished into three lesion types (Fig. 2): 1) type I lesions, affecting subcortical WM and some or all layers of the cortex; 2) type II lesions, ie, very small lesions located within the cortical GM; 3) type III lesions, ie, subpial, usually extensive, lesions affecting cortical layer I (molecular layer) and any number of further cortical layers.

Images of all 48 MBP stained sections were acquired and areas measured of both nonlesional cortex (NLC) and CGML. Area measurements are expressed in mm^2. In type I lesions, only the proportion affecting the cortex was included in the area measurement.

Statistics

For comparison of qMR indices before and after fixation, Student's paired *t*-test used.

This was also applied to estimate the relative dependence of qMR indices on the amount of myelin in the tissue. For this purpose, cases were divided into those with 1) a CGML area (averaged over all blocks of each case) above, and 2) below the median percentage area affected by CGML of the entire sample. This analysis was performed in both unfixed and fixed condition separately. Analysis was carried out using SPSS v. 16 (Chicago, IL).

RESULTS

The mean age of the subjects at death was 58 (SD = 14) years and the mean disease duration was 26 (SD = 11) years. The mean eEDSS score was 8 (SD = 1.1). Figure 3 illustrates the change following fixation of each qMR index in each individual brain slice. The mean values in unfixed and fixed cortical GM were as follows: T_1 was 1156 msec (216) in unfixed condition vs. 617 msec (114) after fixation; MTR (unfixed) was 29.1 pu (2.5) vs. 24.1 pu (3.3) after fixation, and f_B (unfixed) was 3.2 pu (2.3) vs. 5.4 pu (0.7) after fixation (all $P < 0.01$).

Between one and six tissue blocks (mean 3.2; SD = 1.7) were available for each of the 15 brain slices. In the 48 tissue blocks a total of 96 CGML were detected, 17 of which were

type I, 12 were type II, and 67 were type III CGML (Table 1). A mean area fraction of 18.6% of the total cortical GM was affected by demyelination, ranging from zero to 33.8%, except for one outlier, in which 84% of a small block was demyelinated (Table 2).

The median percentage of CGML as a proportion of the total cortical GM area was 12.1%. Hence, cases were divided into groups with high (>12.1%) and low (<12.1%) percentage of CGML. No significant differences were detected between these groups for any qMR index, either before or after fixation (Tables 3).

DISCUSSION

This study revealed two key findings: First, formalin fixation of postmortem MS cortical GM led to significant changes of all three qMR indices investigated. Second, the "myelination status" of the CGM (NLC vs. CGML) did not significantly affect any of the mean qMR values investigated, either before or after fixation.

The mechanisms underlying tissue fixation are not fully understood. Formaldehyde solutions seem to react with functional groups of macromolecules, notably primary amines (eg, lysine) and thiols (eg, cystein), to form crosslinks. Secondary reactions with less reactive groups such as primary amides (eg, glutamine), guanidine groups, and thyrosine ring carbons may also be involved. Intra- and intermolecular crosslinking of macromolecules results in altered physical characteristics of tissues, which can be described as a gel that largely retains the cellular constituents in their topographic in vivo relationships (22,23).

Whereas the effects on qMR indices of formalin fixation on MS WM have been reported previously (11), no such information is available for MS GM. The cellular composition differs significantly between GM vs. WM (12) as do their biochemical constituents. For example, compared to WM, GM consists of significantly more water (84.5% vs. 70% of total weight) and contains less lipids (total lipid content in GM: 5–6.2/100 g vs. 16–22/100 g in WM) (13). It was therefore conceivable that such differences would result in different changes of qMR indices following formalin fixation.

It has been suggested that the effects of formalin fixation on qMR parameters takes up to 5.4 weeks to stabilize (24), attributed, in part, to the slow penetration of the brain samples by formalin solution. Using slices of brain (instead of whole brains) in our study allowed for fast penetration, suggesting it is unlikely that the effect of penetration had any significant impact on our observations.

The distinction between NLC and CGML using clinical MRI systems operating at 1.5T has been shown to be challenging (25). The location and size of CGML, as well as intrinsic properties of NLC and CGML, are not conducive for the separation of these two using MRI because: 1) most CGML affect superficial layers of the cortex. Hence, they are in close contact with the subarachnoid space leading to susceptibility artifacts at the interface between cortex and cerebrospinal fluid (CSF). 2) Although histologically CGML frequently occur as "ribbons" of demyelination, these are often only a few millimeters (or even less) wide, thereby approaching the limits of MR resolution, at least at 1.5T. Intrinsic properties complicating CGML detection include i) the significantly less pronounced inflammatory response compared to WML (26); ii) the lack of blood brain barrier disruption in many CGML (27); and iii) the smaller difference—compared to WML and normal-appearing WM (NAWM)—in relaxation times between CGML and NLC (28). All the above factors may contribute to the lack of contrast on MRI between NLC and CGML. Whereas our study did not specifically aim to improve visibility of CGML, careful visual inspection of the scans was performed. However, no CGML was identified. Hence, our MRI data reflect composites consisting of NLC and CGML, and possibly even remyelinated cortex (29).

Although MRI acquisition was performed using samples at room temperature, the mean T_1, MTR, and f_B obtained in postmortem MS cortex prior to fixation were very similar to values detected in patients with MS (16,30) in vivo, although for f_B in vivo data for comparison were only available of “deep” GM (16). These results are in line with findings from an earlier study of postmortem WM (11) suggesting that changes of T_1, MTR, and f_B inferred from unfixed postmortem MS brain may closely reflect in vivo changes in both cortical GM and WM. It should be noted that the two-point method used to determine T_1 will be inherently less precise than multipoint methods due to the effects of noise; however, the technique has been validated (14) and used in many studies (30,31), indicating that the technique is sufficiently precise to determine subtle changes in T_1.

In our sample T_1 and MTR in the cortical GM dropped to 53% and 82%, respectively, of their prefixation values, which, again, is very similar to the degree these qMR indices decreased in postmortem NAWM following fixation (11). Given that more than 80% of the cortex investigated in this study appeared light-microscopically not affected by demyelination, these results suggest that despite significant differences in the macromolecular composition of GM and WM formalin fixation leads to a near identical dynamic pattern of T_1 and MTR in both tissue compartments. This pattern is in line with the previously reported reduction in T_1 (and hence of MTR) due to 1) the formalin solution itself, and 2) the chemical reactions formalin initiates, ie, crosslinking of macromolecules, which results in a shift of protons from the free pool to the macromolecular pool (32,33).

In contrast to T_1 and MTR—but again similar to its behavior in WM (11)—f_B increased following fixation. Unlike MTR, which is influenced by T_1 (in a simplistic equation MTR can be described as $MTR = T_1 * f_B * k$, where k is a constant) f_B is thought to reflect protons in the macromolecular proton pool only (34,35), and this pool may increase following fixation as protons in soluble macromolecules become protons in insoluble macromolecules.

When comparing cases with high vs. low CGML load the proportion of CGM vs. NLC did not affect the qMR values. This may have been due to 1) an overall low myelin content of the cortex, which even in healthy individuals harbors only ≈10% the amount of myelin in the WM, and 2) less than 19% of the cortex in this study being demyelinated.

Whereas our MRI data did not allow differentiation between MS NLC and CGML, histological assessment revealed demyelination of nearly 19% of the cortex. Lesion type III was the most abundant, making up 62% of the total area of cortical demyelination. The proportion of CGML and NLC was highly variable, ranging from zero to ≈34% (except for one outlier in which 84% of a small block was affected by demyelination).

The number of tissue blocks available for histology per brain slice varied between one and six. Hence, whereas the tissue blocks used in this study provide an indication as to the proportion of NLC and CGML in the brain slice from which blocks were dissected, these data need to be interpreted with caution. Meanwhile, the proportion of NLC vs. CGML in our study was similar to an earlier report based on a much larger sample size (36), suggesting our data is reasonably representative.

In conclusion, the qMR indices T_1, MTR, and f_B in both GM and WM change in the same direction and to a similar degree following formalin fixation, despite significant differences in the cellular and biochemical composition of GM and WM.

Future studies should evaluate the significance of the detected postfixation changes for the inference of specific tissue features (eg, myelin content, neuronal density) in the cortical GM from MRI/pathology correlation studies. For this purpose, ultrahigh-field MRI (3T and

above, potentially enabling distinction between NLC and CGML (37)) and quantitative histology should be employed.

Acknowledgments

We thank Richard Reynolds, Richard Nicholas, Djordje Gveric, and the team of the Multiple Sclerosis Tissue Bank (MSTB) based at Imperial College London (Hammersmith Campus) for provision of the brain samples used in this study.

Contract grant sponsor: Wellcome Trust; Contract grant number: 075941 (to K.S.); Contract grant sponsor: MS Society of Great Britain & Northern Ireland funding to the NMR Research Unit of the UCL Institute of Neurology and the MSTB; Contract grant sponsor: Department of Health's National Institute for Health Research Biomedical Research; Centres funding scheme to the University College London Hospital/UCL.

REFERENCES

1. Compston A, Coles A. Multiple sclerosis. Lancet. 2008; 372:1502–1517. [PubMed: 18970977]
2. Polman CH, Reingold SC, Edan G, et al. Diagnostic criteria for multiple sclerosis: 2005 revisions to the "McDonald Criteria. Ann Neurol. 2005; 58:840–846. [PubMed: 16283615]
3. Miller DH, Weinshenker BG, Filippi M, et al. Differential diagnosis of suspected multiple sclerosis: a consensus approach. Mult Scler. 2008; 14:1157–1174. [PubMed: 18805839]
4. Barkhof F, Calabresi PA, Miller DH, Reingold SC. Imaging outcomes for neuroprotection and repair in multiple sclerosis trials. Nat Rev Neurol. 2009; 5:256–266. [PubMed: 19488083]
5. Bo L, Geurts JJ, Ravid R, Barkhof F. Magnetic resonance imaging as a tool to examine the neuropathology of multiple sclerosis. Neuropathol Appl Neurobiol. 2004; 30:106–117. [PubMed: 15043708]
6. Franklin RJ, ffrench-Constant C. Remyelination in the CNS: from biology to therapy. Nat Rev Neurosci. 2008; 9:839–855. [PubMed: 18931697]
7. Schmierer K, Scaravilli F, Altmann DR, Barker GJ, Miller DH. Magnetization transfer ratio and myelin in postmortem multiple sclerosis brain. Ann Neurol. 2004; 56:407–415. [PubMed: 15349868]
8. MacKay AL, Vavasour IM, Rauscher A, et al. MR relaxation in multiple sclerosis. Neuroimaging Clin N Am. 2009; 19:1–26. [PubMed: 19064196]
9. Barkhof F, Bruck W, De Groot CJ, et al. Remyelinated lesions in multiple sclerosis: magnetic resonance image appearance. Arch Neurol. 2003; 60:1073–1081. [PubMed: 12925362]
10. Shepherd TM, Thelwall PE, Stanisz GJ, Blackband SJ. Aldehyde fixative solutions alter the water relaxation and diffusion properties of nervous tissue. Magn Reson Med. 2009; 62:26–34. [PubMed: 19353660]
11. Schmierer K, Wheeler-Kingshott CA, Tozer DJ, et al. Quantitative magnetic resonance of postmortem multiple sclerosis brain before and after fixation. Magn Reson Med. 2008; 59:268–277. [PubMed: 18228601]
12. Pelvig DP, Pakkenberg H, Stark AK, Pakkenberg B. Neocortical glial cell numbers in human brains. Neurobiol Aging. 2008; 29:1754–1762. [PubMed: 17544173]
13. Davison AN, Wajda M. Analysis of lipids from fresh and preserved adult human brains. Biochem J. 1962; 82:113–117. [PubMed: 13883978]
14. Parker GJ, Barker GJ, Tofts PS. Accurate multislice gradient echo T(1) measurement in the presence of non-ideal RF pulse shape and RF field nonuniformity. Magn Reson Med. 2001; 45:838–845. [PubMed: 11323810]
15. Barker GJ, Tofts PS, Gass A. An interleaved sequence for accurate and reproducible clinical measurement of magnetization transfer ratio. Magn Reson Imaging. 1996; 14:403–411. [PubMed: 8782178]
16. Davies GR, Tozer DJ, Cercignani M, et al. Estimation of the macromolecular proton fraction and bound pool T2 in multiple sclerosis. Mult Scler. 2004; 10:607–613. [PubMed: 15584482]

17. Henkelman RM, Huang X, Xiang QS, Stanisz GJ, Swanson SD, Bronskill MJ. Quantitative interpretation of magnetization transfer. Magn Reson Med. 1993; 29:759–766. [PubMed: 8350718]
18. Ramani A, Dalton C, Miller DH, Tofts PS, Barker GJ. Precise estimate of fundamental in-vivo MT parameters in human brain in clinically feasible times. Magn Reson Imaging. 2002; 20:721–731. [PubMed: 12591568]
19. Plummer DL. Dispimage: a display and analysis tool for medical images. Riv Neuroradiol. 1992; 5:489–495.
20. Mouritzen Dam A. Shrinkage of the brain during histological procedures with fixation in formaldehyde solutions of different concentrations. J Hirnforsch. 1979; 20:115–119. [PubMed: 556570]
21. Peterson JW, Bo L, Mork S, Chang A, Trapp BD. Transected neurites, apoptotic neurons, and reduced inflammation in cortical multiple sclerosis lesions. Ann Neurol. 2001; 50:389–400. [PubMed: 11558796]
22. Fox CH, Johnson FB, Whiting J, Roller PP. Formaldehyde fixation. J Histochem Cytochem. 1985; 33:845–853. [PubMed: 3894502]
23. Hopwood, D. Theory and practice of histological techniques. 4th ed.. Bancroft, JD.; Stevens, A., editors. Churchill Livingstone; New York: 1996. p. 23-45.
24. Yong-Hing CJ, Obenaus A, Stryker R, Tong K, Sarty GE. Magnetic resonance imaging and mathematical modeling of progressive formalin fixation of the human brain. Magn Reson Med. 2005; 54:324–332. [PubMed: 16032673]
25. Geurts JJ, Bo L, Pouwels PJ, Castelijns JA, Polman CH, Barkhof F. Cortical lesions in multiple sclerosis: combined postmortem MR imaging and histopathology. AJNR Am J Neuroradiol. 2005; 26:572–577. [PubMed: 15760868]
26. Bo L, Vedeler CA, Nyland H, Trapp BD, Mork SJ. Intracortical multiple sclerosis lesions are not associated with increased lymphocyte infiltration. Mult Scler. 2003; 9:323–331. [PubMed: 12926836]
27. van Horssen J, Brink BP, de Vries HE, van der Valk P, Bo L. The blood-brain barrier in cortical multiple sclerosis lesions. J Neuropathol Exp Neurol. 2007; 66:321–328. [PubMed: 17413323]
28. Bainbridge, A.; Schmierer, K.; Miller, DH.; Ordidge, RJ.; Yousry, TA. High-field (7T) magnetic resonance imaging of post-mortem multiple sclerosis brain. Proc 12th Annual Meeting ISMRM; Kyoto. 2004. p. 2316
29. Albert M, Antel J, Bruck W, Stadelmann C. Extensive cortical remyelination in patients with chronic multiple sclerosis. Brain Pathol. 2007; 17:129–138. [PubMed: 17388943]
30. Davies GR, Hadjiprocopis A, Altmann DR, et al. Normal-appearing grey and white matter T1 abnormality in early relapsing-remitting multiple sclerosis: a longitudinal study. Mult Scler. 2007; 13:169–177. [PubMed: 17439881]
31. Manfredonia F, Ciccarelli O, Khaleeli Z, et al. Normal-appearing brain T1 relaxation time predicts disability in early primary progressive multiple sclerosis. Arch Neurol. 2007; 64:411–415. [PubMed: 17353385]
32. Nagara H, Inoue T, Koga T, Kitaguchi T, Tateishi J, Goto I. Formalin fixed brains are useful for magnetic resonance imaging (MRI) study. J Neurol Sci. 1987; 81:67–77. [PubMed: 3681342]
33. Macchi G, Cioffi RP. An in vivo and post mortem MRI study in multiple sclerosis with pathological correlation. Ital J Neurol Sci. 1992; 13(Suppl 14):97–103. [PubMed: 1345748]
34. Sled JG, Pike GB. Quantitative imaging of magnetization transfer exchange and relaxation properties in vivo using MRI. Magn Reson Med. 2001; 46:923–931. [PubMed: 11675644]
35. Tofts, PS.; Steens, SCA.; van Buchem, MA. Quantitative MRI of the brain. Measuring changes caused by disease. Tofts, PS., editor. John Wiley & Sons; Chichester , UK: p. 257-98.
36. Bo L, Vedeler CA, Nyland HI, Trapp BD, Mork SJ. Subpial demyelination in the cerebral cortex of multiple sclerosis patients. J Neuropathol Exp Neurol. 2003; 62:723–732. [PubMed: 12901699]
37. Schmierer K, Parkes HG, So P-W, et al. High field (9.4T) magnetic resonance imaging of multiple sclerosis cortical grey matter lesions. Brain. 2010; 133:858–867. [PubMed: 20123726]

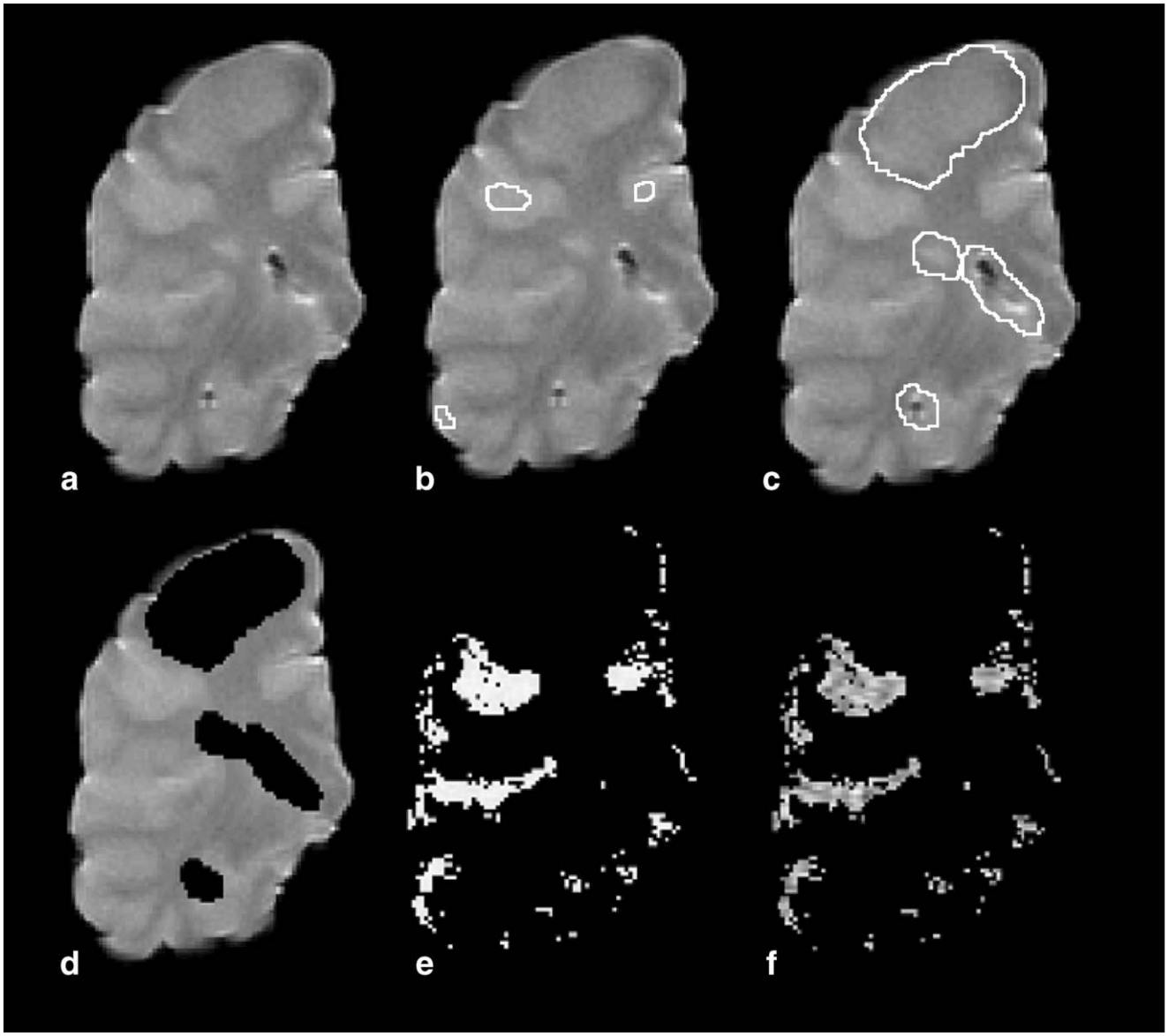

Figure 1. Processing of magnetic resonance images for production of CGM masks.
On T_2-weighted scans **(a)** three ROIs were placed in the CGM **(b)**. From these ROIs the mean and SD were calculated. Areas of non-CGM and white matter lesions **(c)** were removed **(d)**. Subsequently, T_2-weighted images were thresholded to produce CGM masks **(e)**. CGM masks were then applied to quantitative MR maps (in this case MTR) **(f)**. Images shown were acquired in unfixed condition.

Europe PMC Funders Author Manuscripts

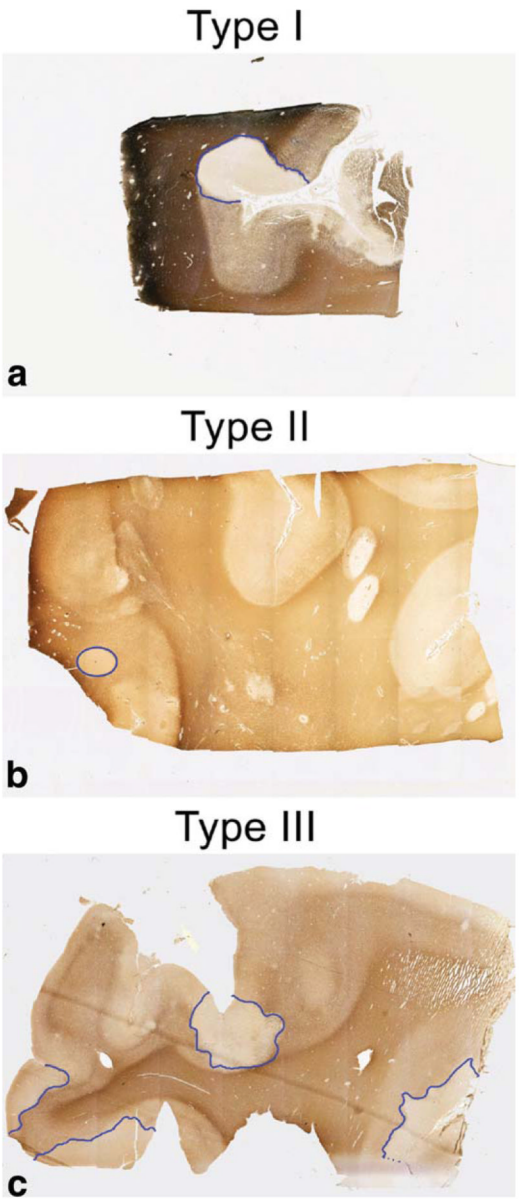

Figure 2. Classification of CGML on sections immunostained for myelin basic protein.
Type I CGML **(a)** affected subcortical WM and some or, as in this case, all layers of the cortex. Type II lesions **(b)** were located entirely within the CGM. Type III **(c)** lesions were subpial CGML affecting the molecular layer I and any further number of cortical layers.

Europe PMC Funders Author Manuscripts

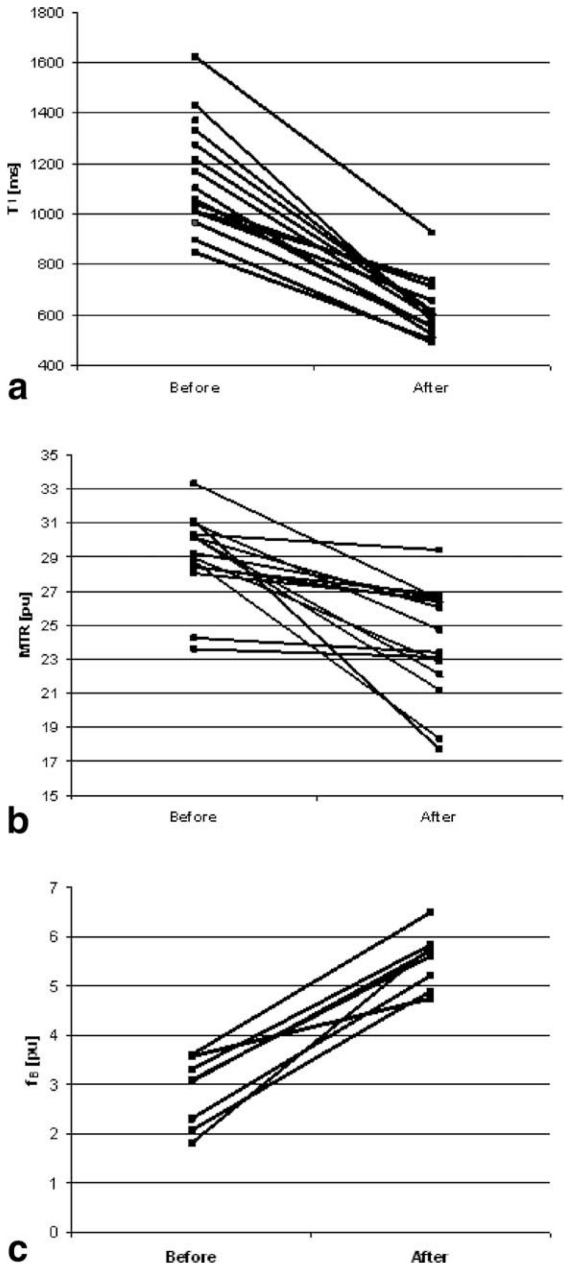

Figure 3. T_1 (a), MTR (b), and f_B (c) in up to 15 postmortem multiple sclerosis brain slices before and after fixation in 10% formalin.

Each line indicates the data and change of an individual case. See text for mean values ($P <$ 0.01 for all comparisons).

Europe PMC Funders Author Manuscripts

Table 1

Cortical Lesion Types in 15 Postmortem Multiple Sclerosis Brain Slices

Case no.	Type I	Type II	Type III	Total number of lesions
1	0	1	0	1
2	0	2	6	8
3	0	0	8	8
4	3	2	8	13
5	0	1	0	1
6	1	0	5	6
7	2	0	8	10
8	2	0	0	2
9	0	0	4	4
10	2	1	10	13
11	0	0	1	1
12	0	0	2	2
13	1	3	0	4
14	6	0	13	19
15	0	2	2	4
All	16	12	62	96

Europe PMC Funders Author Manuscripts

Table 2

Total Cortical Area (Total Area), Area of Nonlesional Cortex (NLC) and of Cortical Gray Matter Lesions (CGML) in 15 Postmortem Multiple Sclerosis Brain Slices*

Case no.	Total area [mm^2]	NLC area [mm^2]	CGML area [mm^2]	NLC [%]	CGML [%]
1	249.2	249.2	0.03	>99.9	<0.1
2	136.2	125.8	10.4	92.4	7.6
3	147.4	122.3	25.1	83.0	17.0
4	392.4	364.6	27.8	92.9	7.1
5	209.4	209.1	0.2	99.9	0.1
6	133.3	117.3	16.0	88.0	12.0
7	93.2	61.8	31.5	66.2	33.8
8	26.8	4.2	22.6	15.6	84.4
9	43.2	34.1	9.1	79.0	21.0
10	171.3	117.7	53.6	68.7	31.3
11	254.1	246	8.1	96.8	3.2
12	56.8	50.0	6.9	87.9	12.1
13	17.8	14.8	3.0	83.1	16.9
14	304.4	224.8	79.6	73.8	26.2
15	101.1	94.9	6.2	93.9	6.1
Sum	2366.7	2036.6	300.10	81.4	18.6

*The two columns on the right describe NLC and CGML as a percentage of the total cortical area.

Europe PMC Funders Author Manuscripts

Table 3

Comparison of MRI Indices in Postmortem Multiple Sclerosis Cortical Gray Matter Between Groups With High (>12.1%) and Low (<12.1%) Percentage of Cortical Gray Matter Lesions (CGML)*

	Index	High CGML mean (SD)	Low CGML mean (SD)	*P*-value
Tissue unfixed	T_1 [ms]	1174 (181)	1137 (265)	0.61
	MTR [pu]	28.1 (2.8)	30.1 (1.7)	0.23
	f_B [pu]	2.8 (0.8)	3.5 (0.8)	0.25
Tissue fixed	T_1 [ms]	570 (45)	680 (151)	0.18
	MTR [pu]	23.7 (3.3)	24.6 (3.5)	0.46
	f_B [pu]	5.5 (0.5)	5.2 (1.0)	0.79

*Values obtained prior to and after fixation. MTR, magnetization transfer ratio; f_B, fraction of macromolecular protons.